

# HybridQ: Hybrid Classical-Quantum Generative Adversarial Network for Skin Disease Image Generation

Qingyue Jiao<sup>1</sup>, Kangyu Zheng<sup>2</sup>, Yiyu Shi<sup>1</sup>, and Zhiding Liang<sup>2</sup>

<sup>1</sup> University of Notre Dame, Notre Dame IN 46556, USA  
qjiao@nd.edu

<sup>2</sup> Rensselaer Polytechnic Institute, Troy NY 12180, USA

**Abstract.** Machine learning-assisted diagnosis is gaining traction in skin disease detection, but training effective models requires large amounts of high-quality data. Skin disease datasets often suffer from class imbalance, privacy concerns, and object bias, making data augmentation essential. While classical generative models are widely used, they demand extensive computational resources and lengthy training time. Quantum computing offers a promising alternative, but existing quantum-based image generation methods can only yield grayscale low-quality images. Through a novel classical-quantum latent space fusion technique, our work overcomes this limitation and introduces the first classical-quantum generative adversarial network (GAN) capable of generating color medical images. Our model outperforms classical deep convolutional GANs and existing hybrid classical-quantum GANs in both image generation quality and classification performance boost when used as data augmentation. Moreover, the performance boost is comparable with that achieved using state-of-the-art classical generative models, yet with over  $25\times$  fewer parameters and  $10\times$  fewer training epochs. Such results suggest a promising future for quantum image generation as quantum hardware advances. Finally, we demonstrate the robust performance of our model on real IBM quantum machine with hardware noise.

**Keywords:** Quantum Machine Learning · Medical Image Generation · Skin Disease Diagnosis.

## 1 Introduction

Common data augmentation techniques include deep learning-based methods, such as convolutional neural networks and generative models, as well as traditional augmentation techniques, such as random cropping, rotation, and flipping [12]. Generative models can be leveraged to produce high-quality generated images, which can be used to augment datasets. Examples of generative models include Generative Adversarial Networks (GANs) [21] and diffusion-based models [5]. While these models have demonstrated promising results in image generation, they still encounter challenges such as long training times and mode

collapse. Quantum computing has recently gained attention for its potential to enhance machine learning, including hybrid classical-quantum GANs which offer promising advantages in optimization and efficiency. Yet limited by the noise and scale of Noisy Intermediate-Scale Quantum (NISQ) hardware, the model capacity of hybrid classical-quantum GANs is significantly smaller than that of classical generative models, restricting their ability to generate realistic images of high complexity.

In this work, we introduce HybridQ, which builds on a novel concept of classical and quantum latent space fusion. It allows the hybrid classical-quantum GAN to mitigate the scalability and noise issues in quantum computers, and for the first time in the literature, enables a quantum computer to generate color medical images that are practically useful. The generated images are evaluated for data augmentation in two skin disease datasets: the ISIC 2019 skin lesion dataset [20] [3] [4] and the Fitzpatrick17k dataset [7] [6]. Both visual and quantitative evaluations demonstrate that compared with classical deep convolutional GANs [17] and state-of-art hybrid classical-quantum GAN MosaiQ [18], HybridQ can generate images with higher quality and more variations. The generated images are then tested in classification tasks to evaluate their augmentation performance, where again HybridQ outperforms the other two. In addition, even with quantum hardware limitations, the precision/recall improvements achieved by HybridQ is comparable with those from the state-of-the-art medical image generative model VQ-MAGE [21], which requires over 25x more parameters and 10x more training time. With rapid advances in quantum hardware error correction and scalability, while not yet exceeding state-of-the-art classical generative model performance, HybridQ holds great potential for fast and efficient high-quality medical image generation in the future. The robustness of HybridQ is evaluated on IBM Brisbane quantum machine.

## 2 Background

Quantum computing, with its unique quantum mechanical properties, such as superposition, entanglement, and parallelism, has sparked significant interest in quantum machine learning. Variational quantum circuits (VQCs) are a fundamental component of quantum machine learning algorithms. The gates in VQCs have tunable parameters and are trained in a hybrid manner by leveraging well-established classical loss functions and optimization techniques.

Hybrid classical-quantum GANs were first introduced in [13], where the authors demonstrated the potential of quantum advantages over classical GANs theoretically. Quantum generators in [11] have shown performance comparable to classical GANs while utilizing 94.98% fewer parameters. The semi-supervised qSGAN [15] indicates that the rich expressibility of quantum generators could potentially solve classification problems that are classically intractable. In pursuit of higher quality image generation, QGPatch [10] and MosaiQ [18] employ quantum sub-generators and dimensionality reduction techniques to enhance the scalability of quantum GANs. Despite the efforts, scalability still remains

a significant challenge: QGPatch [10] operates on  $8 \times 8$  grayscale images, while MosaiQ [18] was evaluated on  $28 \times 28$  grayscale images.

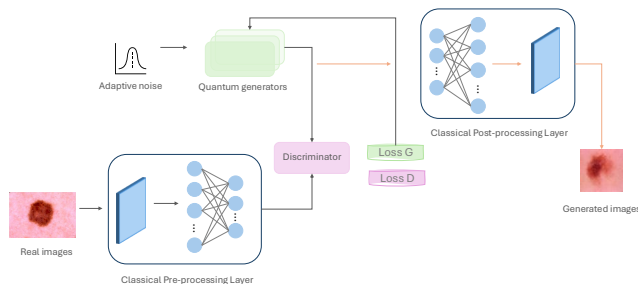


Fig. 1: Workflow of HybridQ. The black arrows indicate the flow of training processing. The orange arrows indicate the flow of inference process.

### 3 Method

#### 3.1 Latent Space-based Training

Figure 1 illustrates the overall structure of HybridQ. To improve scalability, we propose a novel latent space-based training scheme. Instead of training the quantum generators on raw images, we employ a simple yet powerful classical pre-processing layer to transform real images into their latent representations. The pre-processing layer consists of a  $4 \times 4$  convolution, followed by a Leaky Rectified Linear Unit (Leaky ReLU). The feed-forward layers map the flattened output to 100-dimension feature space. We feed an adaptive noise vector with the same latent dimension into the group of quantum generators, as illustrated in Section 3.2. This adaptive noise, updated based on the ratio of training loss between the quantum generator and the classical discriminator, mitigates intra-class mode collapse and improves the variety of generated images [18].

During the inference process, a classical post-processing layer reconstructs images from the quantum output. The classical post-processing layer takes the 100-dimensional output from the quantum generator and decodes it through one feed-forward layer, followed by a ReLU. A  $3 \times 3$  convolution followed by a hyperbolic tangent function (Tanh) outputs the generated image.

This latent space-based training and inference approach mitigates hardware constraints and maximizes the potential of quantum information processing. Previous work [2] has explored latent space-based quantum generators; however, fully quantum GANs—incorporating both quantum generators and quantum discriminators—are difficult to scale. Furthermore, our goal is not to completely discard classical components, which have already demonstrated excellent performance. We aim to synergize the strengths of both classical and quantum

computational power. Such latent space-based scheme enabled us to build the first hybrid classical-quantum GAN for complex color images.

### 3.2 Quantum Generator

In HybridQ, the generator is a hybrid classical-quantum network and the discriminator consists of a classical convolutional neural network [17]. The quantum generator is made up of quantum sub-generators, each implemented as a variational quantum circuit, shown in Fig. 2. The distribution of features over sub-generators both improve scalability and mitigate noise of current quantum hardware. Each variational quantum sub-generator consists of three main components: data encoding gates, trainable quantum gates, and measurement gates. The variational circuit design follows a structure similar to MosaiQ [18], as this shallow, simplistic design provides sufficient expressivity without triggering barren plateau [14], an optimization challenge that arises when quantum circuits become deep. The data encoding block has fixed parameters and encodes classical features as rotation angles into each qubit. The central quantum layer consists of six repetitions of quantum gate groups. The first rotation gate has tunable rotation angles and process information using a single qubit. The following controlled-not (CNOT) gate creates entanglement between consecutive qubits, a unique quantum property that effectively increases the expressivity of quantum circuits. Finally, the measurement gates produce classical outputs in the latent space.

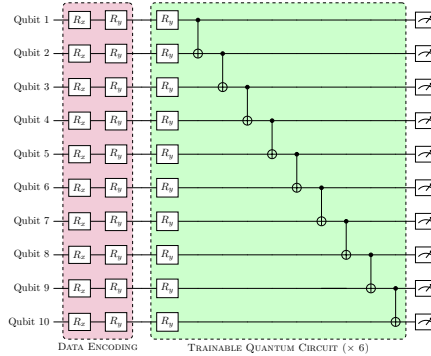


Fig. 2: Variational quantum circuit ansatz design of each quantum sub-generator

## 4 Experiment

### 4.1 Dataset, Metrics and Baselines

HybridQ is evaluated on ISIC 2019, a dermoscopic skin lesion image dataset containing nine diagnostic categories [20] [3] [4], and Fitzpatrick17k, a dermato-

logical skin disease dataset annotated with Fitzpatrick skin type labels [7] [6]. Three categories from ISIC 2019 are used for training and evaluation of the hybrid GAN network: melanoma (MEL), melanocytic nevus (NV), and basal cell carcinoma (BCC). A total of 4114, 11419, and 3317 training samples are used for each class, respectively. The Fitzpatrick17k dataset is split into three higher-level categories: benign (B), malignant (M), and non-neoplastic (NE). 1339, 1357, and 7221 training samples are used for each class, respectively. For both datasets, all images are resized to  $64 \times 64$ . The training samples are separated by class labels, and an unconditional GAN is trained for each class.

The generated images are evaluated by the Fréchet Inception Distance (FID) score [9], which computes the distance between the distributions of real and generated images in a deep feature space. In this work, Inception v3 [19] is used as the feature extractor. Lower FID score represents better generation quality.

To evaluate the effectiveness of data augmentation, we fine-tuned ResNet-50 [8] with varying mixing ratio of real and generated images. The mixing ratio  $\alpha$  is defined as the ratio of generated images in training dataset. Both datasets have an imbalanced number of training samples across classes. We keep the same class distribution and use 10% of the original dataset, augmenting it with generated images. The test images come from the real dataset only. The learning rate for fine-tuning the classification model is set to  $1 \times 10^{-3}$ . The classification performance is evaluated using accuracy (ACC), precision, and recall.

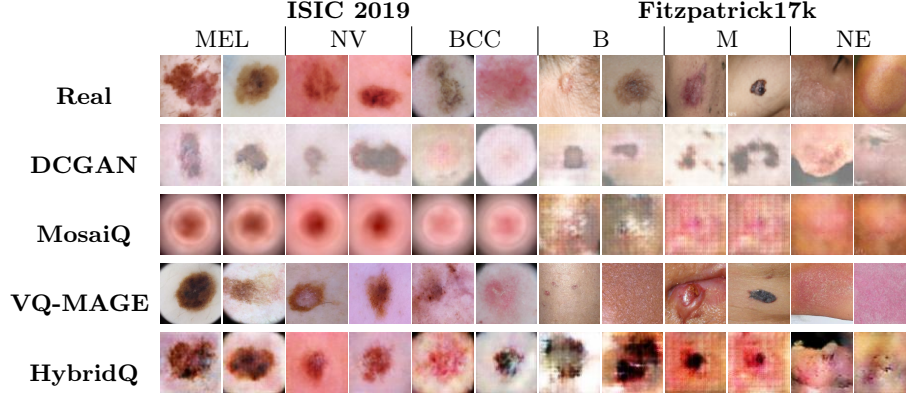


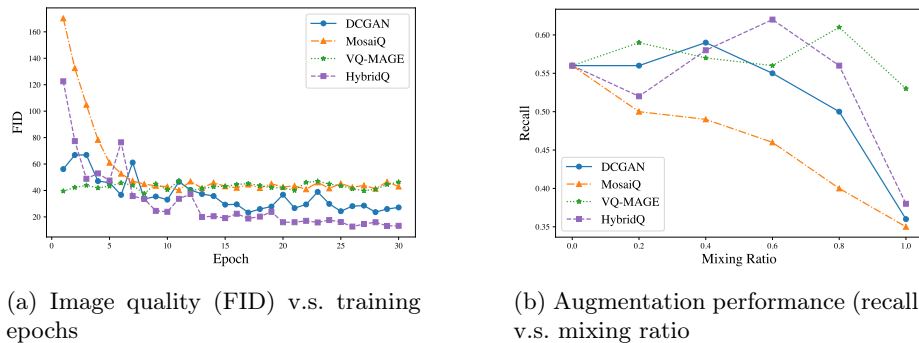
Fig. 3: Visual evaluations of generated images.

The generation and augmentation performance are compared against both classical and quantum generative models. As a classical baseline, we use DCGAN (6.3M parameters), following the implementation in [17]. DCGAN is trained for 100 epochs. MosaiQ [18] (3921 parameters) is the state-of-the-art hybrid quantum GAN network. The original MosaiQ architecture is designed for  $28 \times 28$  grayscale images and consists of 8 quantum sub-generators, each with 5 qubits.

Table 1: FID scores ( $\downarrow$ ) of the images generated for different skin diseases in ISIC 2019 (left) and Fitzpatrick17k (right).

Model	MEL	NV	BCC	Model	B	M	NE
DCGAN [17]	21.23	16.51	19.60	DCGAN [17]	25.16	28.42	26.56
MosaiQ [18]	36.22	53.39	43.00	MosaiQ [18]	36.22	53.39	43.00
VQ-MAGE [21]	10.91	9.88	7.18	VQ-MAGE [21]	7.18	6.99	6.05
HybridQ	14.93	21.76	13.29	HybridQ	18.34	13.29	9.99

To scale up the model, we utilize 10 quantum sub-generators, each with 10 qubits. MosaiQ is trained on IBM’s quantum simulator for 500 epochs. Additionally, a pre-trained VQ-MAGE model with an adapter [21] for medical image generation (around 94M trainable parameters) is used, as it represents state-of-the-art high-quality image generation for medical datasets. The adapter is fine-tuned for 1000 epochs to convergence. Finally, for HybridQ (3.7M parameters), it is trained using PyTorch [16] and PennyLane [1]. Training is completed on IBM’s quantum simulator. Adam optimizer is used and the learning rate is 0.3 for the quantum circuits,  $2 \times 10^{-4}$  for the classical pre-processing and post-processing layers, and  $2 \times 10^{-3}$  for the discriminator. HybridQ is trained for 100 epochs due to IBM quantum simulator limitations.



(a) Image quality (FID) v.s. training epochs

(b) Augmentation performance (recall) v.s. mixing ratio

Fig. 4: Image quality and performance of the classification model fine-tuned with the augmented data, both on Fitzpatrick17k.

## 4.2 Generation Performance

Fig. 3 presents randomly sampled generated images from various models. Table 1 presents the FID scores of each model at the end of training.

We start with the comparison between HybridQ and classical and state-of-the-art hybrid classical-quantum GANs. From Fig. 3, the images produced by DCGAN is obviously blurred, and features are less clear. MosaiQ, the current

state-of-the-art hybrid classical-quantum GAN, fails to generate meaningful images. This is likely due to its use of Principal Component Analysis (PCA) for dimensionality reduction and PCA inverse transformation for reconstructing images from quantum outputs. While PCA works well for smaller grayscale images, it results in information loss for more complex datasets. HybridQ, with classical pre-processing and post-processing layers, retains sufficient information. The generated images show clear features that closely resemble real images in each class and are less blurred compared to DCGAN. However, the generation quality is not as good for the Fitzpatrick17k dataset. Since Fitzpatrick17k contains images of human body parts and have smaller number of training samples, it is more challenging to learn distributions across classes. This is particularly evident in the images generated for the benign and malignant classes. For non-neoplastic images, which have significantly more training samples, HybridQ successfully generates images that resemble real ones.

Quantitatively, HybridQ achieves lower FID score than DCGAN in all but one class and achieves consistently lower FID than MosaiQ. To further investigate the training process of classical and quantum GANs, Fig. 4(a) shows the FID scores over the first 30 training epochs for different methods on Fitzpatrick17k. From the figure we can see that the FID scores stabilize the fastest with HybridQ. This suggests that quantum GANs has the potential to speedup learning. As quantum hardware continues to advance, the benefits and speedup of quantum models will likely become more pronounced in image generation. Moreover, from Table 1, for classes with limited training samples, such as the benign (B) and malignant (M) classes in Fitzpatrick17k, HybridQ also has superior performance, demonstrating its capability to learn distributions effectively from a smaller number of real images.

Next, we compare HybridQ with state-of-the-art classical medical image generative model VQ-MAGE. From Fig. 3, the pre-trained VQ-MAGE model presents the best overall results; this is also validated from the results in Table 1. Notably, VQ-MAGE utilizes a pre-trained MAGE model and further fine-tunes the model with an adapter. This training and fine-tuning process requires a significant amount of data as well as computational resources as reflected in Fig. 4(a). Simply fine-tuning the adapter takes 1000 epochs to converge, while HybridQ is trained from scratch using only 100 epochs, a 10 $\times$  reduction.

Table 2: Accuracy, precision and recall of classification model fine-tuned using data generated by different methods.

	ISIC 2019			Fitzpatrick17k		
	ACC (%)	Precision	Recall	ACC (%)	Precision	Recall
No Aug.	71.67	0.62	0.56	56.89	0.56	0.56
DCGAN [17]	73.67	0.67	0.68	60.00	0.60	0.59
MosaiQ [18]	70.06	0.56	0.62	51.25	0.49	0.50
VQ-MAGE [21]	76.22	0.74	0.71	61.33	0.62	0.61
HybridQ	74.67	0.72	0.70	61.22	0.62	0.62

### 4.3 Augmentation Performance

To verify the effectiveness of the generated images in augmenting medical datasets and improving diagnostic results, we fine-tune ResNet-50 with different mixing ratios of generated images from each method and real images. Fig. 4(b) demonstrates the change of classification recall as we vary the ratio of generated images  $\alpha$  in training dataset for Fitzpatrick17k. From the figure we can see that the performance increases first as the number of training samples increases, but the score starts to drop when the generated images make up the majority of training dataset. Table 2 presents the accuracy, precision, and recall of the fine-tuned ResNet-50 using the optimal mixing ratio on both datasets.

We first compare HybridQ with classical and state-of-the-art hybrid classical-quantum GANs. From Table 2, HybridQ achieves the highest performance gain compared with DCGAN and MosaiQ. Since MosaiQ fails to generate high-quality images, it negatively impacts the performance. Compared with ResNet-50 fine-tuned using real data only, mixing images generated by HybridQ yields 3% and 4.33% accuracy increase on ISIC 2019 and Fitzpatrick17k, respectively. HybridQ also improves the precision by 0.10 and 0.06 and the recall by 0.14 and 0.06 on ISIC 2019 and Fitzpatrick17k, respectively.

Next, we compare HybridQ with state-of-the-art medical image generative model VQ-MAGE. From Table 2, while VQ-MAGE achieves slightly higher accuracy gain than HybridQ, both yield nearly identical improvements in precision and recall, which are key metrics for imbalanced datasets. Note again that VQ-MAGE uses a pre-trained MAGE model that is  $25\times$  larger than HybridQ and it takes  $10\times$  more epochs to train the adapter than that used to train HybridQ from scratch.

### 4.4 HybridQ on Real NISQ Computers

Finally, the classical neural layers in HybridQ not only helps scalability but also mitigates the noise of real quantum hardware. To see this, we run the trained HybridQ to generate skin disease images on IBM’s backend machine Brisbane, which has 127 qubits. The generated images achieve FID scores of 23.25, 24.76, 15.59, 21.65, 18.75, and 10.25 for MEL, NV, BCC in ISIC 2019 and B, M and NE in Fitzpatrick17k, respectively. Compared with those obtained from quantum simulators in Table 1, the FID scores do not increase by a significant amount.

## 5 Conclusion

In this work, we present HybridQ, a novel hybrid classical-quantum GAN designed for skin disease image generation and dataset augmentation. HybridQ is the first hybrid classical-quantum GAN capable of generating complex color images. As quantum hardware continues to advance in error correction and scale up, quantum-enhanced medical image processing will provide benefits in more real-world medical imaging applications.



## References

1. Bergholm, V., Izaac, J., Schuld, M., Gogolin, C., Ahmed, S., Ajith, V., Alam, M.S., Alonso-Linaje, G., AkashNarayanan, B., Asadi, A., Arrazola, J.M., Azad, U., Banning, S., Blank, C., Bromley, T.R., Cordier, B.A., Ceroni, J., Delgado, A., Matteo, O.D., Dusko, A., Garg, T., Guala, D., Hayes, A., Hill, R., Ijaz, A., Isacsson, T., Ittah, D., Jahangiri, S., Jain, P., Jiang, E., Khandelwal, A., Kottmann, K., Lang, R.A., Lee, C., Loke, T., Lowe, A., McKiernan, K., Meyer, J.J., Montañez-Barrera, J.A., Moyard, R., Niu, Z., O’Riordan, L.J., Oud, S., Panigrahi, A., Park, C.Y., Polatajko, D., Quesada, N., Roberts, C., Sá, N., Schoch, I., Shi, B., Shu, S., Sim, S., Singh, A., Strandberg, I., Soni, J., Száva, A., Thabet, S., Vargas-Hernández, R.A., Vincent, T., Vitucci, N., Weber, M., Wierichs, D., Wiersema, R., Willmann, M., Wong, V., Zhang, S., Killoran, N.: PennyLane: Automatic differentiation of hybrid quantum-classical computations (2022), <https://arxiv.org/abs/1811.04968>
2. Chang, S.Y., Thanasilp, S., Saux, B.L., Vallecorsa, S., Grossi, M.: Latent style-based quantum gan for high-quality image generation (2024), <https://arxiv.org/abs/2406.02668>
3. Codella, N.C.F., Gutman, D., Celebi, M.E., Helba, B., Marchetti, M.A., Dusza, S.W., Kalloo, A., Liopyris, K., Mishra, N., Kittler, H., Halpern, A.: Skin lesion analysis toward melanoma detection: A challenge at the 2017 international symposium on biomedical imaging (isbi), hosted by the international skin imaging collaboration (isic) (2018), <https://arxiv.org/abs/1710.05006>
4. Combalia, M., Codella, N.C.F., Rotemberg, V., Helba, B., Vilaplana, V., Reiter, O., Carrera, C., Barreiro, A., Halpern, A.C., Puig, S., Malvey, J.: Bcn20000: Dermoscopic lesions in the wild (2019), <https://arxiv.org/abs/1908.02288>
5. Dhariwal, P., Nichol, A.: Diffusion models beat gans on image synthesis. In: Proceedings of the 35th International Conference on Neural Information Processing Systems. NIPS ’21, Curran Associates Inc., Red Hook, NY, USA (2021)
6. Groh, M., Harris, C., Daneshjou, R., Badri, O., Koochek, A.: Towards transparency in dermatology image datasets with skin tone annotations by experts, crowds, and an algorithm. Proceedings of the ACM on Human-Computer Interaction **6**(CSCW2), 1–26 (2022)
7. Groh, M., Harris, C., Soenksen, L., Lau, F., Han, R., Kim, A., Koochek, A., Badri, O.: Evaluating deep neural networks trained on clinical images in dermatology with the fitzpatrick 17k dataset. In: Proceedings of the IEEE/CVF Conference on Computer Vision and Pattern Recognition. pp. 1820–1828 (2021)
8. He, K., Zhang, X., Ren, S., Sun, J.: Deep residual learning for image recognition. In: Proceedings of the IEEE Conference on Computer Vision and Pattern Recognition (CVPR). pp. 770–778. IEEE (2016). <https://doi.org/10.1109/CVPR.2016.90>
9. Heusel, M., Ramsauer, H., Unterthiner, T., Nessler, B., Hochreiter, S.: Gans trained by a two time-scale update rule converge to a local nash equilibrium. In: Proceedings of the 31st International Conference on Neural Information Processing Systems. p. 6629–6640. NIPS’17, Curran Associates Inc., Red Hook, NY, USA (2017)
10. Huang, H.L., Du, Y., Gong, M., Zhao, Y., Wu, Y., Wang, C., Li, S., Liang, F., Lin, J., Xu, Y., Yang, R., Liu, T., Hsieh, M.H., Deng, H., Rong, H., Peng, C.Z., Lu, C.Y., Chen, Y.A., Tao, D., Zhu, X., Pan, J.W.: Experimental quantum generative adversarial networks for image generation. Physical Review Applied **16**(2) (Aug 2021). <https://doi.org/10.1103/physrevapplied.16.024051>, <http://dx.doi.org/10.1103/PhysRevApplied.16.024051>

11. Huang, K., et al.: Quantum generative adversarial networks with multiple superconducting qubits. *npj Quantum Inf.* **7**, 165 (2021). <https://doi.org/10.1038/s41534-021-00503-1>
12. Liu, C., Fan, F., Schwarz, A., Maier, A.: Cut to the Mix: Simple Data Augmentation Outperforms Elaborate Ones in Limited Organ Segmentation Datasets . In: proceedings of Medical Image Computing and Computer Assisted Intervention – MICCAI 2024. vol. LNCS 15008. Springer Nature Switzerland (October 2024)
13. Lloyd, S., Weedbrook, C.: Quantum generative adversarial learning. *Phys. Rev. Lett.* **121**, 040502 (Jul 2018). <https://doi.org/10.1103/PhysRevLett.121.040502>, <https://link.aps.org/doi/10.1103/PhysRevLett.121.040502>
14. McClean, J.R., Boixo, S., Smelyanskiy, V.N., Babbush, R., Neven, H.: Barren plateaus in quantum neural network training landscapes. *Nature Communications* **9**(1), 4812 (Nov 2018). <https://doi.org/10.1038/s41467-018-07090-4>, <https://doi.org/10.1038/s41467-018-07090-4>
15. Nakaji, K., Yamamoto, N.: Quantum semi-supervised generative adversarial network for enhanced data classification. *Scientific Reports* **11**(1) (Oct 2021). <https://doi.org/10.1038/s41598-021-98933-6>, <http://dx.doi.org/10.1038/s41598-021-98933-6>
16. Paszke, A., Gross, S., Massa, F., Lerer, A., Bradbury, J., Chanan, G., Killeen, T., Lin, Z., Gimelshein, N., Antiga, L., Desmaison, A., Kopf, A., Yang, E., DeVito, Z., Raison, M., Tejani, A., Chilamkurthy, S., Steiner, B., Fang, L., Bai, J., Chintala, S.: Pytorch: An imperative style, high-performance deep learning library. In: Wallach, H., Larochelle, H., Beygelzimer, A., d'Alché-Buc, F., Fox, E., Garnett, R. (eds.) *Advances in Neural Information Processing Systems*. vol. 32. Curran Associates, Inc. (2019)
17. Radford, A., Metz, L., Chintala, S.: Unsupervised representation learning with deep convolutional generative adversarial networks (2016), <https://arxiv.org/abs/1511.06434>
18. Silver, D., Ranjan, A., Patel, T., Gandhi, H., Cutler, W., Tiwari, D.: Mo-saiQ: Quantum Generative Adversarial Networks for Image Generation on NISQ Computers . In: 2023 IEEE/CVF International Conference on Computer Vision (ICCV). pp. 7007–7016. IEEE Computer Society, Los Alamitos, CA, USA (Oct 2023). <https://doi.org/10.1109/ICCV51070.2023.00647>, <https://doi.ieeeecomputersociety.org/10.1109/ICCV51070.2023.00647>
19. Szegedy, C., Vanhoucke, V., Ioffe, S., Shlens, J., Wojna, Z.: Rethinking the inception architecture for computer vision (2015), <https://arxiv.org/abs/1512.00567>
20. Tschandl, P., Rosendahl, C., Kittler, H.: The ham10000 dataset, a large collection of multi-source dermatoscopic images of common pigmented skin lesions. *Scientific Data* **5** (2018), <https://api.semanticscholar.org/CorpusID:263789934>
21. Yuan, Z., Fang, Z., Huang, Z., Wu, F., Yao, Y.F., Li, Y.: Adapting Pre-trained Generative Model to Medical Image for Data Augmentation . In: proceedings of Medical Image Computing and Computer Assisted Intervention – MICCAI 2024. vol. LNCS 15005. Springer Nature Switzerland (October 2024)